Nano Res. 2012, 5(3): 181–189
DOI 10.1007/s12274-012-0198-1
Research Article

ISSN 1998-0124
CN 11-5974/O4

# Facile Syntheses and Enhanced Electrocatalytic Activities of Pt Nanocrystals with {*hkk*} High-Index Surfaces

Lei Zhang, Dingqiong Chen, Zhiyuan Jiang (✉), Jiawei Zhang, Shuifen Xie, Qin Kuang, Zhaoxiong Xie (✉), and Lansun Zheng

Department of Chemistry and State Key Laboratory of Physical Chemistry of Solid Surfaces, College of Chemistry and Chemical Engineering, Xiamen University, Xiamen 361005, China

Received: 8 November 2011 / Revised: 27 December 2011 / Accepted: 30 December 2011


## ABSTRACT

Platinum (Pt) is an outstanding catalyst for many important industrial products. Because of its high cost and scarce reserves, it is very important to improve the performance of Pt catalysts. As the metal nanocrystals (NCs) with high-index surfaces usually show very good catalytic activity because of their high density of atomic steps and kinks, the preparation of Pt NCs with high-index facets has become a very important and hot research topic recently. In this article, we report a facile synthesis of high-yield Pt NCs with a series of {*hkk*} high-index facets including {211} and {411} via a solvothermal method using Pt(Ⅱ) acetylacetonate as the Pt source, 1-octylamine as the solvent and capping agent, and formaldehyde as an additional surface structure regulator. Multipod Pt NCs with dominant {211} side surfaces were produced without formaldehyde, while concave Pt NCs with dominant {411} surfaces formed under the influence of formaldehyde. By analyzing the products by IR spectroscopy, we found the presence of CO on the surface of concave Pt NCs with {411} surfaces prepared from the solution containing formaldehyde. It was concluded that amine mainly stabilized the monoatomic step edges, resulting in the {211} exposed surface; with addition of formaldehyde, it decomposed into CO, leading to the formation of {411} surfaces by the additional adsorption of the CO on the {100} terraces. In addition, it was found that the as-prepared Pt NCs with high-index {211} and {411} surfaces exhibited much better catalytic activity in the electro-oxidation of ethanol than a commercial Pt/C catalyst or Pt nanocubes with low-index {100} surfaces, and the catalytic activities of Pt crystal facets decreased in the sequence {411}>{211}>{100}.

## KEYWORDS

Pt nanocrystals, surface structure, high-index facets, structure–property relationship, electrocatalysis, crystal growth

## 1. Introduction

Platinum (Pt) is an outstanding catalyst for many important industrial products [1–4]. Because of its high cost and rare reserves, it is very important to improve the performance of Pt catalysts. It is well known that the performance of a crystalline catalyst in heterogeneous catalytic processes depends markedly on the exposed crystal facets and usually the high-index facets of fcc metals exhibit higher catalytic activities due to their high density of atomic steps, ledges, kinks, and dangling bonds [5–8]. However, most shape-controlled

Address correspondence to Zhiyuan Jiang, zyjiang@xmu.edu.cn; Zhaoxiong Xie, zxxie@xmu.edu.cn

synthetic methods result in Pt nanocrystals (NCs) bounded by low-index facets, such as {111} and {100} facets [1–4, 9–16], since the high-index facets usually disappear during the crystal growth because of their high surface energies. The breakthrough in the synthesis of Pt NCs with high-index facets was realized by an electrochemical method using a square-wave potential technique [17, 18]. However, electrochemical methods are not suitable for large scale synthesis. Since our first report of the preparation of well-shaped gold NCs with high-index surfaces by wet chemical synthesis [19], several groups also demonstrated the possibility of employing conventional solution-based methods in the growth of gold, palladium and gold@palladium NCs with high-index facets [20–29]. To date, there have only been a few reports concerning the preparation of Pt NCs with high-index facets by conventional chemical syntheses, which could be due to the Pt–Pt bond energy being much larger than that of gold or palladium, and its surface energy being not easy to modify via weak interactions with normal surfactants. Very recently, Xia and co-workers reported the synthesis of Pt concave nanocubes with {530} high-index facets by employing a Pt pyrophosphato complex as the precursor [30]. In addition, Zheng and co-workers reported the preparation of concave polyhedral Pt NCs with {411} facets by using $H_2PtCl_6$ as precursor, an amine as surface controller, poly(vinylpyrrolidone) (PVP) as the surfactant and *N*,*N*-dimethylformamide (DMF) as solvent [31]. In Zheng's work, different kinds of amines, such as ethylamine and *n*-butylamine, all induced the formation of {411} facets. However, the role of the amine in the formation of {411} facets is still unclear because of the employment of PVP and DMF. In this paper, we report the syntheses of high-yield Pt NCs with {*hkk*} high-index facets including {211} and {411} via a simple solvothermal method using Pt(Ⅱ) acetylacetonate ($Pt(acac)_2$) as the Pt source, 1-octylamine as the solvent and capping agent, and formaldehyde as an additional surface structure regulator. It was concluded that the amine stabilized the monoatomic step edges, resulting in the {211} exposed surface; the by-product CO additionally stabilized the {100} terraces, leading to the formation of {411} surfaces. In addition, it was found that the as-prepared Pt NCs with dominant high-index {211} and {411} surfaces exhibited much better catalytic activity than a commercial Pt/C catalyst or Pt nanocubes with low-index {100} surfaces, and the catalytic activities of Pt crystal facets decreased in the sequence {411}> {211}>{100}.

## 2. Experimental

### 2.1 Materials

$Pt(acac)_2$ (99%), 1-octylamine (99%) and Pt/C were purchased from Alfa Aesar, formaldehyde solution (40%) was purchased from Sinopharm Chemical Reagent Co. Ltd. (Shanghai, China). All reagents were used as received without further purification.

### 2.2 Synthesis of multipod Pt NCs

In a typical synthesis, $Pt(acac)_2$ (5.0 mg) was mixed together with 10 mL of 1-octylamine. The resulting homogeneous yellow solution was transferred to a 25 mL Teflon-lined stainless-steel autoclave. The sealed vessel was then heated at 200 ℃ for 3 h before it was cooled to room temperature. The black products were separated via centrifugation and further purified by an ethanol-acetone (2∶1) mixture three times.

### 2.3 Synthesis of concave Pt NCs

$Pt(acac)_2$ (5.0 mg) and 0.05 mL of formaldehyde solution (40%) were mixed together with 10 mL of 1-octylamine. The resulting homogeneous yellow solution was transferred to a 25 mL Teflon-lined stainless-steel autoclave. The sealed vessel was then heated at 200 ℃ for 5 h before it was cooled to room temperature. The black products were separated via centrifugation and further purified by an ethanol-acetone (2∶1) mixture three times.

### 2.4 Structural characterization

The morphology and structure of the products were characterized by scanning electron microscopy (SEM, S-4800), transmission electron microscopy (TEM, JEM-2100) and X-ray powder diffraction (XRD, PANalytical X'Pert diffractometer with Cu Kα radiation). The samples for IR spectra measurements (Nicolet 330) were obtained by depositing the ethanol suspensions

of Pt NCs on a KBr substrate followed by solvent evaporation.

### 2.5 Electrochemical measurements

A glassy carbon electrode (diameter of 5 mm) was carefully polished and washed before every experiment. The ethanol suspensions of the as-prepared Pt NCs or Pt/C were dripped onto the surface of the glassy carbon electrode and dried at room temperature. The cyclic voltammetry (CV) measurements were carried out using an electrochemical workstation (CHI 631a, Shanghai Chenhua Co., China). A Pt sheet and a standard calomel electrode (SCE) were employed as the counter and reference electrodes, respectively. All the electrode potentials in this paper are quoted versus the SCE. The glassy carbon electrode loaded with the as-prepared Pt NCs or Pt/C was electrochemically cleaned by continuous potential cycling between –0.20 and 0.80 V at 100 mV/s until a stable cyclic voltammogram curve was obtained. The electrochemical reactivity and electrochemically active surface area of the catalysts were determined by the area of the hydrogen desorption peaks in the cyclic voltammetry measurement performed in 0.5 mol/L $H_2SO_4$ electrolyte at a scan rate of 50 mV/s (25 ˚C).

## 3. Results and discussion

Figure 1(a) shows a typical SEM image of the product prepared by directly reducing $Pt(acac)_2$ with 1-octylamine, indicating that large quantity of multipods was successfully synthesized in a high yield. By investigating the SEM images carefully, it can be found that most of the multipods have eight bunches of nanorods growth along the diagonal lines of the cube (Fig. 1(b)). The surfaces of these nanorods seem smooth, and each rod has a diameter of about 5 nm and a length in the range of 30–100 nm. The structure and phase of the as-prepared NCs was confirmed by XRD patterns (Fig. 1(c)) to be pure face-centered cubic (fcc) metallic Pt (JCPDS 04-0802).

The structural features of the as-prepared multipod Pt NCs were then further revealed by TEM images and selected area electron diffraction (SAED) patterns. A typical TEM image (Fig. 2(a)) shows that the multipod NCs consisted of several bunches of straight

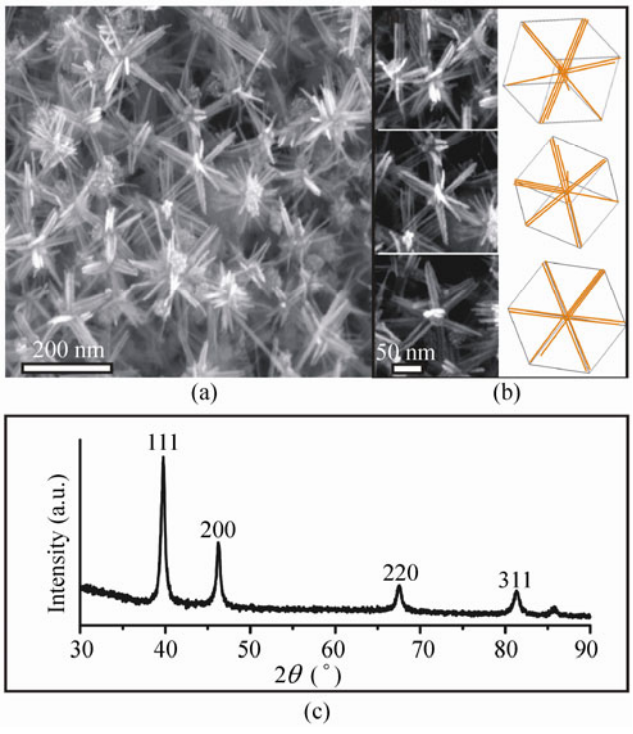


**Figure 1** (a) Typical SEM image of the products prepared by reducing $Pt(acac)_2$ in 1-octylamine, (b) A series of high-magnification SEM images and corresponding models of the multipod NCs observed in different orientations. (c) XRD patterns of as-prepared multipod Pt NCs

nanorods along different directions. Each nanorod (Fig. 2(b)) was single crystal as suggested by the SAED pattern (Fig. 2(c)). The whole multipod (Fig. 2(d)) also had single-crystal-like features (Fig. 2(e)), indicating that all the nanorod bunches were well oriented. In addition, we found that the cross-sections of the individual nanorod had a hexagonal shape, as clearly demonstrated by some individual pods oriented along the electron beam direction as shown in Fig. 2(f). The corresponding SAED patterns (Fig. 2(g)) revealed that the side surfaces of the single pod were perpendicular to the <211> direction and therefore they were {211} facets. To further confirm the presence of high-index {211} facets, when the multipod was surveyed along the $[01\bar{1}]$ zone axes, the high resolution TEM (HRTEM) image (Fig. 2(h)) clearly showed that the surface consists of two-atomic-length {111} terraces and monoatomic {100} steps, which corresponds to a perfect {211} facet. For comparison, the schematic model of the (211) surface projected in the same direction is shown in Fig. 2(i), and is consistent with the HRTEM

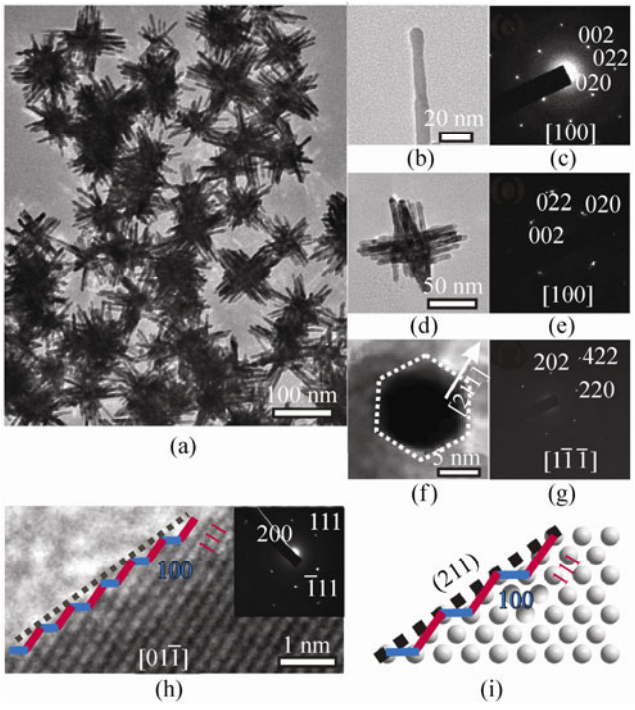


**Figure 2** TEM images of (a) a large quantity of multipod Pt NCs; (b) TEM image and (c) corresponding SAED patterns of a single nanorod; (d) TEM image and (e) corresponding SAED patterns of an individual multipod Pt NCs; (f) cross-section image and (g) the corresponding SAED patterns of an individual nanorod projected along the [1$\bar{1}\bar{1}$] direction. (h) HRTEM image of the edge region of the nanorod projected along the [01$\bar{1}$] direction, showing the atomic arrangements of the surface. (i) Atomic model of the Pt (211) surface projected from the [01$\bar{1}$] direction, showing that the (211) surface is a combination of (111) terraces and (100) steps

images. Therefore, it can be concluded that the dominant side surfaces of the as-prepared multipod Pt NCs are {211} facets.

Interestingly, the morphology and surface structures of the Pt NCs can be easily tailored by adding small amounts of formaldehyde to the reaction system. When 0.05 mL of formaldehyde solution (40%) was introduced into 10 mL of growth solution, instead of multipod NCs, the product in high yield was concave Pt NCs as shown in Figs. 3(a) and 3(b). By investigating the images carefully, three typical outlines of these particles can be observed as shown in Figs. 3(c)–3(h). The corresponding SAED patterns (Figs. 3(i)–3(k)) recorded by directing the electron beam on whole individual Pt NCs indicated that the concave Pt NCs are single crystals, rather than multiply twinned crystals. Combining the SEM and TEM images and

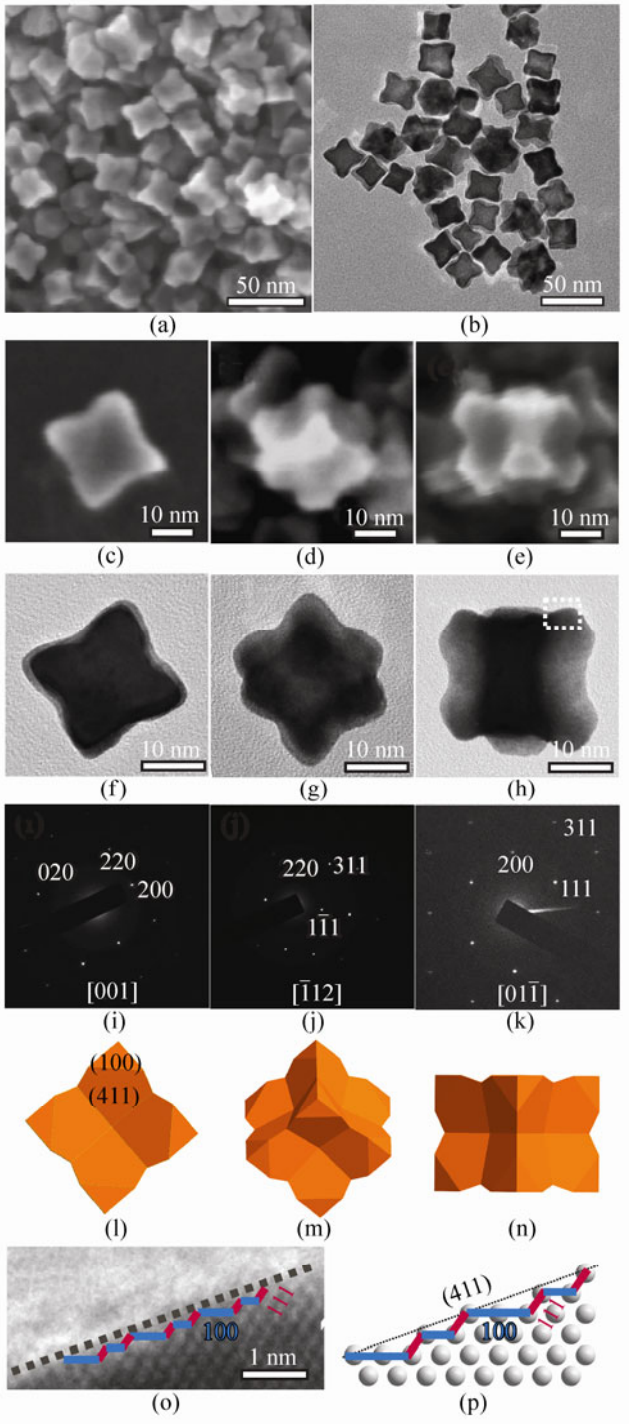


**Figure 3** Representative SEM image (a) and TEM image (b) of the products in the presence of formaldehyde. (c)–(n) A series of enlarged SEM images, TEM images, corresponding SAED patterns and models of the concave Pt NCs in different orientations. (o) HRTEM image of the edge region marked with a box in Fig. 3(h), showing the atomic arrangements of the surface. (p) Atomic model of the Pt(411) surface projected along the [01$\bar{1}$] direction, showing that the (411) surface is a combination of (100) terraces and (111) steps

related indexed SAED patterns, we may conclude that these NCs have same geometrical character and can be regarded as concave NCs with eight triangular pyramids grown along the eight body diagonal directions of a cube, but with different orientations. A proposed schematic model of the concave Pt NCs is shown in Figs. 3(l)–3(n). In this model, the inclined planes of the triangular pyramids are expected to be {*hkk*} facets, which consist of (100) terraces and (111) steps. To match the schematic model with the observed concave cube, the inclined surfaces are proposed to be {411} surfaces in the present case. The presence of {411} facets can be confirmed by the HRTEM images (Fig. 3(o)) recorded along the [01$\bar{1}$] zone axes. In addition to the {411} facets, small facets parallel to the surface of an ideal cube can also be observed on the tip of the triangular pyramid, which are the {100} facets.

The presence of high-index surfaces on the as-prepared multipod Pt NCs and concave Pt NCs can be confirmed by surface sensitive electrochemical reactions [32–34]. Figure 4 shows the CV traces of the as-prepared products in 0.50 mol/L $H_2SO_4$ solution. As a comparison, the CV trace of Pt nanocubes with exposed {100} facets [35] is also presented. It can be found that CV traces in the hydrogen adsorption/desorption region exhibit clear a butterfly feature, which shows peaks at –0.14 V, 0.00 V, and 0.08 V. The H-desorption peak at 0.08 V corresponds to Pt(100) terrace sites (long-range-order (100) sites), while the peak at 0.00 V is characteristic of Pt(100) edges and corner surface sites (short-range-order (100) sites) [34]. For the perfect Pt nanocubes (Fig. 4(a)), there is an obvious H-desorption peak at 0.08 V, corresponding to the atomic structure of (100) surfaces. For the multipod Pt NCs (Fig. 4(b)), there is a small peak at about 0.00 V and no peak at 0.08 V, indicating that only short-range-order (100) sites are present on the surface of Pt multipods. Moreover, a small peak emerges at 0.24 V (marked with dotted box in the insert of Fig. 4(b)), which is characteristic of (111) ordered surface domains, can be observed. This result also proves that the multipod Pt NCs contain a small amount (111) terraces, consistent with the atomic structure of the {211} surface. For the concave Pt NCs with {411} facets (Fig. 4(c)), the peak at 0.08 V appears as a weak shoulder peak, indicating the presence of a small amount of long-range-order (100) terraces. The peak at 0.00 V is strong, indicating the concave Pt NCs are rich in Pt(100) terrace edges and corners, which is consistent with the presence of {411} facets and small {100} facets on the concave Pt NCs. It should be mentioned that the peak at –0.14 V has often been thought to be mainly caused by step structures (such as (110)) on the high-index surfaces [32]. It was also

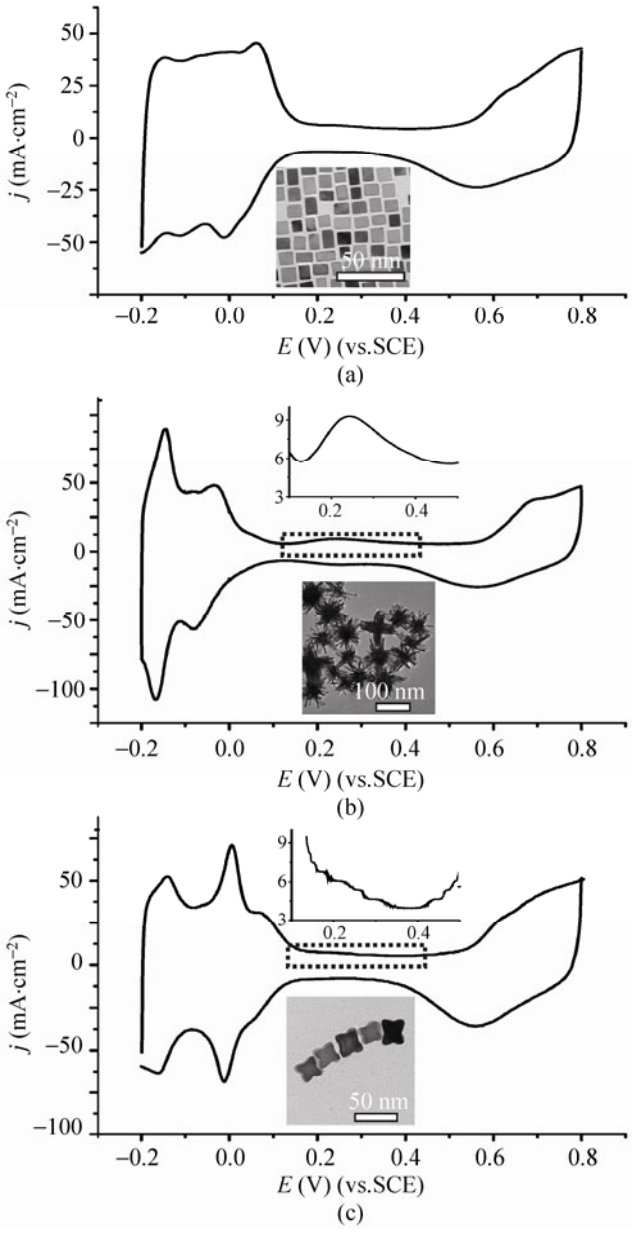


**Figure 4** Cyclic voltammogram of (a) the Pt nanocube, (b) the multipod Pt NCs and (c) concave Pt NCs obtained in 0.50 mol/L $H_2SO_4$. Scan rate: 50 mV/s. The insert is a typical TEM image of the products

reported that such a step structure could be observed at the regions near the corners of the Pt nanoparticles surrounded by low-index facets [36]. Therefore, the intense peak at –0.14 V for both the concave Pt NCs and multipod Pt NCs indicates both of them have many steps and narrow terraces on the surface, which is in good agreement with the atomic structures of {411} and {211} surface.

Recently, Zheng et al. reported the synthesis of Pt NCs with {411} surfaces [31]. They found the addition of short chain amines resulted in the formation of {411} surfaces, and suggested that the amine might stabilize the steps on the {411} surface. However, they used DMF as the solvent and PVP as the additive. The chemical reactions in such an environment, especially after the formation of Pt nuclei, could be complicated because of the high catalytic activity of Pt NCs. In our case, much simpler reactants are introduced, which makes it possible to get a deeper insight into the role of the organic amine in the formation of high-index {*hkk*} surfaces.

It is found that pure 1-octylamine leads to the formation of multipod Pt NCs with dominant {211} surfaces, while the addition of formaldehyde results in the formation of {411} surfaces. Structurally, the {211} surface is different from the {411} surface as shown in the schematic models in Figs. 2(i) and 3(p), respectively. The {211} surface consists of two-atomic-length {111} terraces and monoatomic {100} steps, while the {411} surface is made of {100} terraces and monoatomic {111} steps. Therefore, more information about the influence of the amine and formaldehyde on the surface structure should be revealed.

To investigate the role of the 1-octylamine and formaldehyde, both Pt multipods and concave cubic Pt NCs were analyzed by IR spectroscopy (Fig. 5). The peak located at about 1389 $cm^{-1}$ is assigned to C–N stretching mode of the adsorbed organic amine. The peak located at about 3429 $cm^{-1}$ is assigned to O–H stretching of $H_2O$ and that at 1622 $cm^{-1}$ to O–H bending of $H_2O$. Interestingly, we find a peak located at 2087 $cm^{-1}$ from the concave Pt NCs, while this peak was negligible in the spectrum of the multipod Pt NCs. According to the literature, the peak at 2087 $cm^{-1}$ can be attributed to linearly adsorbed CO [35]. Previous studies showed that the CO preferentially adsorbs on

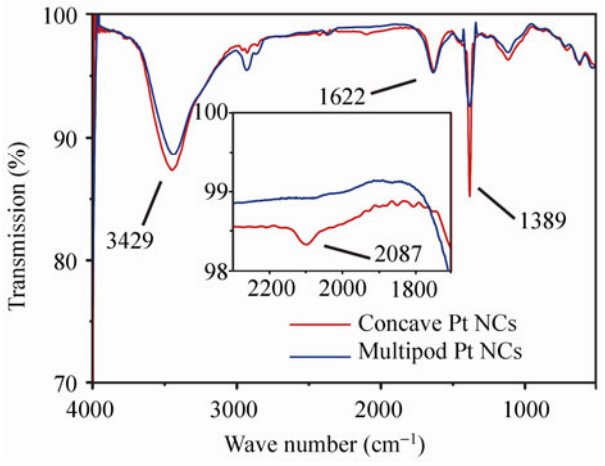


**Figure 5** IR spectra of the as-prepared concave Pt NCs and the multipod Pt NCs

the {100} surface [35]. Therefore, it can be concluded that pure amine preferentially adsorbs on monoatomic step edges consisting of (111) terraces and (100) steps, resulting in the {211} exposed surface, whilst the by-product CO from formaldehyde will stabilize the {100} terraces, and thus enlarge the area of {100} terraces, leading to the formation of {411} surfaces.

To further elucidate the formation process of multipod Pt NCs and concave Pt NCs with high-index surfaces, the products formed after 1 h were studied by TEM. In the case of preparation of multipod NCs mainly exposing {211} surfaces formed in the absence of formaldehyde, we found the primary products at the early reaction stage (after 1 h of reaction) were attached Pt NCs as shown in Fig. 6(a). Therefore, at the beginning, multiple nuclei clusters were formed, and then crystals grew quickly along the <111> direction with exposed high energy {211} surfaces. The formation process for the concave cubic Pt NCs with predominant {411} surfaces differs slightly from that for the multipod NCs. In the presence of formaldehyde, the primary products in the initial reaction stage were free-standing cuboctahedral Pt NCs (Fig. 6(b)). These primary Pt NCs might catalyze the decomposition of formaldehyde into CO, and then concave Pt NCs with mainly exposed {411} surfaces form by the co-adsorption of amine and CO as the reaction time is prolonged.

The role of formaldehyde can be further demonstrated by varying the amount of formaldehyde. Perfect

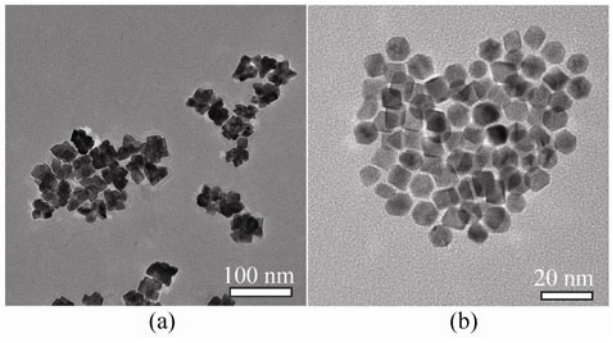


**Figure 6** TEM image of 1 h products (a) without formaldehyde and (b) in the presence of formaldehyde

concave cubes with mainly {411} surfaces were prepared with using 0.05 mL formaldehyde in a total volume of 10 mL of growth solution. When only 0.02 mL formaldehyde was added, the products were a mixture of multipods and concave cubes (Fig. 7(a)). If the amount of formaldehyde was increased to 0.5 mL in a total volume of 10 mL growth solution, the concave structure tended to become flatter and some nanocubes appeared among the products (Fig. 7(b)). This phenomenon can be explained by adsorption of CO, as adding more formaldehyde produced higher concentrations of CO, leading to more stable {100} terraces.

As suggested by the structure features revealed by the TEM observation and the CV traces, the concave Pt NCs and multipod Pt NCs present a high density of Pt atomic steps on their surfaces. They should have high chemical activity. The electro-oxidation of ethanol was used as a probe reaction to examine the electrocatalytic activity of the as-prepared Pt NCs. For comparison, Pt nanocubes and a commercially available Pt/C material were chosen as the reference catalysts. The electrochemically active surface areas of the catalysts were normalized by the area of the hydrogen desorption peaks. Figure 8 shows CVs of ethanol oxidation in a mixture of 0.10 mol/L $HClO_4$ and 0.10 mol/L ethanol at a scan rate of 50 mV/s, using the as-prepared concave Pt NCs, multipod Pt NCs, Pt nanocubes and the commercial Pt/C as working electrodes. In the anodic sweep, the peak at 0.65 V can be attributed to the formation of $CO_2$ and the peak at 1.05 V attributed to the formation of $CH_3CHO$ [37]. During the cathodic sweep, an oxidation peak appears at 0.4 V due to the complete desorption of oxygen from the Pt-surface [38]. It can be found that the concave Pt NCs exhibit the highest electrocatalytic activity among the four catalysts. The peak current density of ethanol oxidation measured on the concave Pt NCs catalysts is three times more than that with the commercial Pt/C catalyst, while the electrocatalytic activity of the Pt nanocubes (consisting of {100} surfaces) is comparable to that of the commercial Pt/C sample. Multipod Pt NCs also showed better catalytic activity than that of Pt nanocubes and the commercial Pt/C, but not as good as that of the concave Pt NCs. Therefore the catalytic activities of Pt NC surfaces decrease in the sequence {411}>{211}>{100}. From the structural point of view, besides the monoatomic steps,

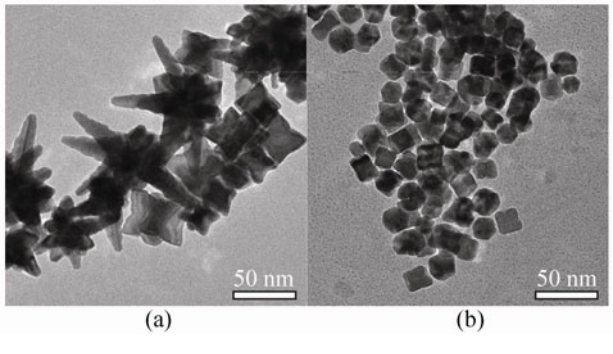


**Figure 7** TEM images of the products obtained with (a) 0.02 mL and (b) 0.5 mL of formaldehyde in total 10 mL reaction solutions. The reaction time was 5 h

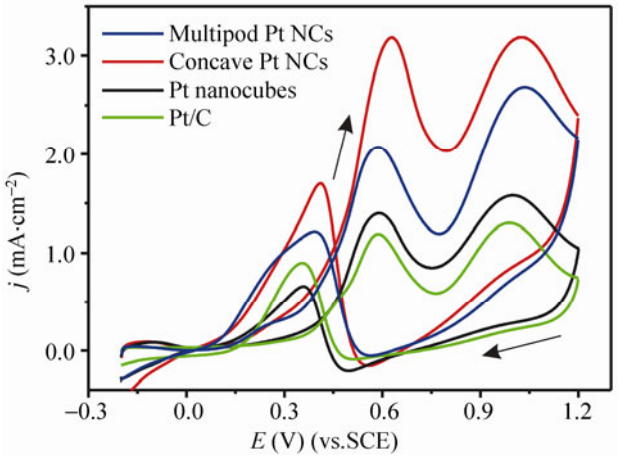


**Figure 8** Electrocatalytic properties of the concave Pt NCs, the multipod Pt NCs, the Pt nanocubes and commercial Pt/C for ethanol oxidation in a mixture of 0.10 mol/L ethanol and 0.10 mol/L $HClO_4$ at 25 ˚C

the {211} surface consists of the most stable {111} terraces, while the {411} surface is constructed of the next most stable {100} terraces. Therefore, the {411} surfaces should be more active than the {211} surfaces, which explains the order of catalytic activity.

## 4. Conclusions

Multipod Pt NCs with dominant {211} high-index surfaces have been successfully synthesized via a facile solvothermal method at 200 ℃, using $Pt(acac)_2$ as platinum precursor, 1-octylamine as the solvent and capping agents. Concave Pt NCs mainly exposing {411} facets were prepared with the help of formaldehyde as an additional surface structure regulator. Pure amine tends to stabilize the monoatomic step edges, resulting in the {211} exposed surface, while the co-adsorption of amine and CO molecules formed by decomposition of formaldehyde makes the {100} terraces more stable, resulting in the exposed {411} surfaces. Due to their high density of surface atomic steps, as-prepared Pt NCs exhibited much better catalytic activity than a commercial Pt/C sample and Pt nanocubes with low-index facets toward the ethanol electro-oxidation. The catalytic activities of Pt NC surfaces decrease in the sequence {411}>{211}>{100}.

## Acknowledgements

This work was supported by the National Basic Research Program of China (Grant No. 2011CBA00508), the National Natural Science Foundation of China (Grant Nos. 21131005, 21021061, 21073145, and 21171141), the National Fund for Fostering Talents of Basic Science (Grant No. J1030415), and the Key Scientific Project of Fujian Province of China (Grant No. 2009HZ0002-1).

## References

[1] Peng, Z. M.; Yang, H. Designer platinum nanoparticles: Control of shape, composition in alloy, nanostructure and electrocatalytic property. *Nano Today* **2009**, *4*, 143–164.

[2] Chen, J. Y.; Lim, B.; Lee, E. P.; Xia, Y. N. Shape-controlled synthesis of platinum nanocrystals for catalytic and electrocatalytic applications. *Nano Today* **2009**, *4*, 81–95.

[3] Chen, A. C.; Holt-Hindle, P. Platinum-based nanostructured materials: Synthesis, properties, and applications. *Chem. Rev.* **2010**, *110*, 3767–3804.

[4] Cheong, S. S.; Watt, J. D.; Tilley, R. D. Shape control of platinum and palladium nanoparticles for catalysis. *Nanoscale* **2010**, *2*, 2045–2053.

[5] Pimentel, G. C. *Opportunities in Chemistry*; National Academy Press: Washington, D. C., 1985; pp 193–265.

[6] Tian, N.; Zhou, Z. Y.; Sun, S. G. Platinum metal catalysts of high-index surfaces: From single-crystal planes to electrochemically shape-controlled nanoparticles. *J. Phys. Chem. C* **2008**, *112*, 19801–19817.

[7] Jiang, Z. Y.; Kuang, Q.; Xie, Z. X.; Zheng, L. S. Syntheses and properties of micro/nanostructured crystallites with high-energy surfaces. *Adv. Funct. Mater.* **2010**, *20*, 3634–3645.

[8] Zhou, Z. Y.; Tian, N.; Li, J. T.; Broadwell, I.; Sun, S. G. Nanomaterials of high surface energy with exceptional properties in catalysis and energy storage. *Chem. Soc. Rev.* **2011**, *40*, 4167–4185.

[9] Teranishi, T.; Kurita, R.; Miyake, M. Shape control of Pt nanoparticles. *J. Inorg. Organomet. Polym.* **2000**, *10*, 145–156.

[10] Herricks, T.; Chen, J. Y.; Xia, Y. N. Polyol synthesis of platinum nanoparticles: Control of morphology with sodium nitrate. *Nano Lett.* **2004**, *4*, 2367–2371.

[11] Elechiguerra, J. L.; Larios-Lopez, L.; Jose-Yacaman, M. Controlled synthesis of platinum submicron and nanometric particles with novel shapes. *Appl. Phys. A* **2006**, *84*, 11–19.

[12] Ren, J. T.; Tilley, R. D. Preparation, self-assembly, and mechanistic study of highly monodispersed nanocubes. *J. Am. Chem. Soc.* **2007**, *129*, 3287–3291.

[13] Maksimuk, S.; Teng, X. W.; Yang, H. Roles of twin defects in the formation of platinum multipod nanocrystals. *J. Phys. Chem. C* **2007**, *111*, 14312–14319.

[14] Demortière, A.; Launois, P.; Goubet, N.; Albouy, P. A.; Petit, C. Shape-controlled platinum nanocubes and their assembly into two-dimensional and three-dimensional superlattices. *J. Phys. Chem. B* **2008**, *112*, 14583–14592.

[15] Ren, J. T.; Tilley, R. D. Shape-controlled growth of platinum nanoparticles. *Small* **2007**, *3*, 1508–1512.

[16] Lim, S. I.; Ojea-Jiménez, I.; Varon, M.; Casals, E.; Arbiol, J.; Puntes, V. Synthesis of platinum cubes, polypods, cuboctahedrons, and raspberries assisted by cobalt nanocrystals. *Nano Lett.* **2010**, *10*, 964–973.

[17] Tian, N.; Zhou, Z. Y.; Sun, S. G.; Ding, Y.; Wang, Z. L. Synthesis of tetrahexahedral platinum nanocrystals with high-index facets and high electro-oxidation activity. *Science* **2007**, *316*, 732–735.

[18] Zhou, Z. Y.; Huang, Z. Z.; Chen, D. J.; Wang, Q.; Tian, N.; Sun, S. G. High-index faceted platinum nanocrystals supported on carbon black as highly efficient catalysts for ethanol electrooxidation. *Angew. Chem. Int. Ed*. **2010**, *49*, 411–414.

[19] Ma, Y. Y.; Kuang, Q.; Jiang, Z. Y.; Xie, Z. X.; Huang, R. B.; Zheng, L. S. Synthesis of trisoctahedral gold nanocrystals with exposed high-index facets by a facile chemical method *Angew. Chem. Int. Ed*. **2008**, *47*, 8901–8904.

[20] Ming, T.; Feng, W.; Tang, Q.; Wang, F.; Sun, L. D.; Wang, J. F.; Yan, C. H. Growth of tetrahexahedral gold nanocrystals with high-index facets. *J. Am. Chem. Soc.* **2009**, *131*, 16350–16351.

[21] Zhang, J.; Langille, M. R.; Personick, M. L.; Zhang, K.; Li, S. Y.; Mirkin, C. A. Concave cubic gold nanocrystals with high-index facets *J. Am. Chem. Soc.* **2010**, *132*, 14012–14014.

[22] Yu, Y.; Zhang, Q. B.; Lu, X. M.; Lee, J. Y. Seed-mediated synthesis of monodisperse concave trisoctahedral gold nanocrystals with controllable sizes *J. Phys. Chem. C* **2010**, *114*, 11119–11126.

[23] Li, J.; Wang, L. H.; Liu, L.; Guo, L.; Han, X. D.; Zhang, Z. Synthesis of tetrahexahedral Au nanocrystals with exposed high-index surfaces. *Chem. Commun.* **2010**, *46*, 5109–5111.

[24] Lu, C. L.; Prasad, K. S.; Wu, H. L.; Ho, J. A. A.; Huang, M. H. Au nanocube-directed fabrication of Au–Pd core–shell nanocrystals with tetrahexahedral, concave octahedral, and octahedral structures and their electrocatalytic activity. *J. Am. Chem. Soc.* **2010**, *132*, 14546–14553.

[25] Yu, Y.; Zhang, Q. B.; Liu, B.; Lee, J. Y. Synthesis of nanocrystals with variable high-index Pd facets through the controlled heteroepitaxial growth of trisoctahedral Au templates. *J. Am. Chem. Soc.* **2010**, *132*, 18258–18265.

[26] Wang, F.; Li, C. H.; Sun, L. D.; Wu, H. S.; Ming, T.; Wang, J. F.; Yu, J. C.; Yan, C. H. Heteroepitaxial growth of high-index-faceted palladium nanoshells and their catalytic performance. *J. Am. Chem. Soc.* **2011**, *133*, 1106–1111.

[27] Jiang, Q. N.; Jiang, Z. Y.; Zhang, L.; Lin, H. X.; Yang, N.; Li, H.; Liu, D. Y.; Xie, Z. X.; Tian, Z. Q. Synthesis and high electrocatalytic performance of hexagram shaped gold particles having an open surface structure with kinks. *Nano Res.* **2011**, *4*, 612–622.

[28] Zhang, J. W.; Zhang, L.; Xie, S. F.; Kuang, Q.; Han, X. G.; Xie, Z. X.; Zheng, L. S. Synthesis of concave palladium nanocubes with high-index surfaces and high electrocatalytic activities. *Chem. Eur. J.* **2011**, *17*, 9915–9919.

[29] Niu, W. X.; Xu, G. B. Crystallographic control of noble metal nanocrystals. *Nano Today* **2011**, *6*, 265–285.

[30] Yu, T.; Kim, D. Y.; Zhang, H.; Xia, Y. Platinum concave nanocubes with high-index facets and their enhanced activity for oxygen reduction reaction. *Angew. Chem. Int. Ed*. **2011**, *50*, 2773–2777.

[31] Huang, X. Q.; Zhao, Z. P.; Fan, J. M.; Tan, Y. M.; Zheng, N. F. Amine-assisted synthesis of concave polyhedral platinum nanocrystals having {411} high-index facets. *J. Am. Chem. Soc.* **2011**, *133*, 4718–4721.

[32] Kim, C.; Lee, H. Shape effect of Pt nanocrystals on electrocatalytic hydrogenation. *Catal. Commun*. **2009**, *11*, 7–10.

[33] Nakamura, M.; Hanioka, Y.; Ouchida, W.; Yamada, M. Hoshi, N. Estimation of surface structure and carbon monoxide oxidation site of shape-controlled Pt nanoparticles. *ChemPhysChem* **2009**, *10*, 2719–2724.

[34] Sun, S. G.; Zhou, Z. Y. Surface processes and kinetics of $CO_2$ reduction on Pt(100) electrodes of different surface structure in sulfuric acid solutions. *Phys. Chem. Chem. Phys.* **2001**, *3*, 3277–3283.

[35] Wu, B. H.; Zheng, N. F.; Fu, G. Small molecules control the formation of Pt nanocrystals: A key role of carbon monoxide in the synthesis of Pt nanocubes. *Chem. Commun.* **2011**, *47*, 1039–1041.

[36] Wang, Z. L.; Ahmad, T. S.; El-Sayed, M. A. Steps, ledges and kinks on the surfaces of platinum nanoparticles of different shapes. *Surf. Sci.* **1997**, *380*, 302–310.

[37] Hitmi, H.; Belgsir, E. M.; Leger, J. M.; Lamy, C.; Lezna, R. O. A kinetic analysis of the electro-oxidation of ethanol at a platinum electrode in acid medium. *Electrochim. Acta* **1994**, *39*, 407–415.

[38] Abd-el-latif, A. A.; Mostafa, E.; Huxter, S.; Attard, G.; Baltruschat, H. Electrooxidation of ethanol at polycrystalline and platinum stepped single crystals: A study by differential electrochemical mass spectrometry. *Electrochim. Acta* **2010**, *55*, 7951–7960.